Locally Disordered Conformer of the Hamster Prion Protein: A Crucial Intermediate to PrP^{Sc}?†

Kazuo Kuwata,‡ Hua Li,§ Hiroaki Yamada,§ Giuseppe Legname,|| Stanley B. Prusiner,||,⊥,@ Kazuyuki Akasaka,*,§,# and Thomas L. James*,@,+

Department of Biochemistry and Biophysics, School of Medicine, Gifu University, 40 Tsukasa-machi, Gifu 500-8705, Japan, Department of Molecular Science, Graduate School of Science and Technology, Kobe University, 1-1 Rokkodai-cho, Nada-ku, Kobe 657-8501, Japan, and Departments of Neurology, Biochemistry and Biophysics, and Pharmaceutical Chemistry and Institute for Neurodegenerative Diseases, University of California, San Francisco, California 94946-0446

Received May 15, 2002; Revised Manuscript Received August 2, 2002

ABSTRACT: A crucial step for transformation of the normal cellular isoform of the prion protein (PrP^C) to the infectious prion protein (PrP^{Sc}) is thought to entail a previously uncharacterized intermediate conformer, PrP*, which interacts with a template PrP^{Sc} molecule in the conversion process. By carrying out $^{15}N-^{1}H$ two-dimensional NMR measurements under variable pressure on Syrian hamster prion protein rPrP(90−231), we found a metastable conformer of PrP^C coexisting at a population of ∼1% at pH 5.2 and 30 °C, in which helices B and C are preferentially disordered. While the identity is still unproven, this observed metastable conformer is most logically PrP* or a closely related precursor. The structural characteristics of this metastable conformer are consistent with available immunological and pathological information about the prion protein.

Prions cause neurodegenerative disorders, manifesting as sporadic, inherited, and infectious illnesses in humans and animals (*1*). In contrast to viruses and viroids, prions lack nucleic acid but are composed of a modified host-encoded glycoprotein denoted PrP^{Sc}.[1] Through a post-translational process, PrP^{Sc} is formed from the normal, cellular isoform denoted PrP^C. Both PrP^C and PrP^{Sc} possess a C-terminal glycosylphosphatidylinositol anchor, a disulfide linking C179 and C214, and are glycosylated at N181 and N197, but no covalent chemical differences between the two isoforms have been found (*2*). Although both isoforms are chemically identical, they possess very different physicochemical properties. PrP^C is mostly α-helical, but PrP^{Sc} has ∼40% β-sheet (*3*, *4*). PrP^C is readily degraded by proteases, but limited proteolysis of PrP^{Sc} yields an N-terminally truncated protein comprised of residues 90−231, which retains infectivity (*5*).

Detailed solution structures of mouse (*6*), hamster (*7*−*9*), bovine (*10*), and human (*11*) recombinant proteins folded to resemble PrP^C immunologically and spectroscopically have been determined by NMR. Although there are small structural differences that may relate to a species barrier to the PrP^C to PrP^{Sc} conversion, the structures are similar in that residues 128−231 constitute a globular fold with three α-helices and a small, imperfectly formed and conformationally flexible β-sheet, the N-terminal segment up to residue 113 is completely disordered, and, at least in the hamster species, residues 113−128 form a hydrophobic cluster with multiple interconverting conformers (*9*). The hydrophobic cluster packs against the core structure.

PrP^{Sc} formation requires the substrate PrP^C to bind to the product PrP^{Sc} at an intermediate stage in the conversion process (*12*). PrP^C is apparently in equilibrium with a metastable intermediate, designated PrP*, which binds to PrP^{Sc} in the conversion (*13*). Indeed, destabilization of PrP^C is necessary for PrP* binding to PrP^{Sc} in vitro (*14*, *15*). Knowledge about the structure of the metastable intermediate and the conformational equilibrium involved is critical for understanding the mechanism of $PrP^C \rightarrow PrP^{Sc}$ transformation but to date has not been available.

† Supported by Grants-in-Aid for Scientific Research from the Ministry of Education, Culture, Sports, Science and Technology of Japan and the Virtual System Laboratory at Gifu University, as well as by grants from the National Institutes of Health and a gift from the G. Harold and Leila Y. Mathers Foundation.

* To whom correspondence should be addressed. E-mail: james@picasso.ucsf.edu. Telephone: (415) 476-1916. Fax: (415) 502-4690.

‡ Gifu University.

§ Kobe University.

|| Department of Neurology, University of California.

⊥ Department of Biochemistry and Biophysics, University of California.

@ Institute for Neurodegenerative Diseases, University of California.

Present address: Department of Biotechnological Science, Faculty of Biology-Oriented Science and Technology, Kinki University, 930 Nishimitani, Uchida-cho, Wakayama 649-6493, Japan.

+ Department of Pharmaceutical Chemistry, University of California.

[1] Abbreviations: PrP, prion protein; PrP^{Sc}, infectious PrP isoform; PrP^C, cellular PrP isoform; PrP*, metastable intermediate PrP isoform; PrP^U, unfolded PrP isoform; rPrP(90−231), recombinant protein commensurate with the N-terminally truncated protease-resistant core of PrP^{Sc}, which retains scrapie infectivity; Mo, mouse; Hu, human; SHa, Syrian hamster; BSE, bovine spongiform encephalopathy; 1D, one-dimensional; 2D, two-dimensional; NOESY, nuclear Overhauser effect spectroscopy; TOCSY, total correlation spectroscopy; HSQC, heteronuclear single-quantum coherence; $I(p)$, cross-peak intensities at pressure p; f_N, fraction of native protein; b^H or b^N, linear component of the chemical shift change with pressure for each amide ^1H or ^{15}N signal, respectively; c^H or c^N, nonlinear component of the chemical shift change with pressure for each amide ^1H or ^{15}N signal, respectively; p, pressure in bars or kilobars.

10.1021/bi026129y CCC: $22.00
Published on Web 09/18/2002

A powerful new method for examining protein structure and equilibrium over a wide conformational space is high-pressure NMR with the on-line cell (*16*). Heteronuclear two-dimensional NMR with a pressure-resisting quartz cell (*17*) enables residue-specific changes in structure (*18*, *19*), dynamics (*20*), and folding (*21*). Pressure directly and efficiently perturbs the conformational equilibrium of proteins in solution by utilizing the volume difference between respective conformers (*16*). It increases the population of rare conformers with respect to that of the abundant conformer under closely physiological solution conditions. A shift in the conformational equilibrium within the folded manifold is normally manifested by nonlinear chemical shift changes with pressure (*22*). A shift involving a larger conformational change is normally detected as discrete changes in signal intensities often with the emergence of new signals (*23*). In the work presented here, we applied the on-line cell, high-pressure NMR method to rPrP(90−231) at pH 5.2 in the pressure range from 30 to 2500 bar at various temperatures. We found a metastable locally disordered conformer of rPrP(90−231) coexisting in solution and characterized its stability and structural features by NMR spectroscopy. This locally disordered conformer is quite likely PrP*, the interactive intermediate essential for PrP^{Sc}.

MATERIALS AND METHODS

Recombinant PrP. Expression, isotopic labeling, purification, and considerations for proper refolding of recombinant Syrian hamster prion protein rPrP(90−231) have been described previously (*7*, *24*). Purified rPrP(90−231), labeled uniformly with ^{15}N, was lyophilized before refolding. Samples were analyzed by mass spectroscopy, circular dichroism, and Fourier transform infrared spectroscopy to ensure the refolded rPrP(90−231) resembles PrP^{C}, i.e., is largely α-helical.

NMR Measurements. The on-line high-pressure NMR system has the protein solution in a quartz tube cell that endures pressures of ≥2500 bar (*18*). The cell was connected to a high-pressure line via frictionless Teflon pistons that separate the protein solution from the pressure mediator (kerosene) in a separator cylinder (BeCu). The cell body (inner diameter of 1 mm, outer diameter of 3 mm) is positioned in a commercial 5 mm NMR probe (Bruker). Pressure was regulated to a desired value between 1 and 2500 bar with a remote handpump and maintained at that value during signal accumulation. For 1D and 2D NMR measurements, samples were dissolved in 95% $^{1}H_2O$ and 5% $^{2}H_2O$ containing 20 mM sodium acetate (pH 5.2) to make a 1 mM protein solution. For chemical shift references, trace amounts of sodium 3-(trimethylsilyl)[2,2,3,3,-^{2}H]tetradeuteriopropionate (TSP-d_4) and dioxane were added to the solution. The dioxane resonance remains unchanged with pressure (3.750 ppm from TSP at 1 bar). As conditions were incrementally changed, chemical shifts could be followed using the assignments previously reported (*9*). In addition to the 3D NOESY-HSQC spectrum, a TOCSY-HSQC spectrum was obtained at 2 °C, to aid with spectral assignments. Tables showing the ^{1}H and ^{15}N chemical shifts as a function of pressure are included in the Supporting Information.

Thermodynamic Analysis. Pressure-induced change in the conformational equilibrium was analyzed assuming a two-state transition

$$\mathrm{N} \Leftrightarrow \mathrm{I} \tag{1}$$

where N represents a native conformer and I represents an intermediate conformer. The two-state assumption pertains to the local environment of each proton or amide group, the intensity of each signal representing the fraction of the native conformer at each site. Normalized cross-peak intensities (I) representing the population of the native conformation at individual sites were fitted to the following equation to obtain changes in free energy (ΔG), partial molar volume (ΔV), compressibility ($\Delta\beta$) associated with the pressure-induced unfolding, and the ambient pressure (P_0):

$$\frac{I(p)}{I(30)} = \frac{1}{1 + \exp\left(-\dfrac{\Delta G}{RT}\right)} = f_{\mathrm{N}} \tag{2}$$

$$\Delta G = \Delta G_0 + \Delta V(P - P_0) - V\left(\frac{\Delta\beta}{2}\right)(P - P_0)^2 \tag{3}$$

where $I(p)$, $I(30)$, and f_N are the cross-peak intensities at pressure p and 30 bar and the fraction of native protein, respectively. ΔG_0 is the Gibbs free energy at ambient pressure. For analysis of unfolding of individual amide residues using HSQC spectra, we ignored the $\Delta\beta$ term in eq 3.

The pressure dependence of the chemical shifts was analyzed according to

$$\delta_i = a_i + b_i p + c_i p^2 \tag{4}$$

where δ_i is the chemical shift for the ith residue and a_i, b_i, and c_i are independent, linear, and nonlinear coefficients of the pressure-induced shift, respectively.

Curve fitting was performed using SigmaPlot 2001 (SPSS Science, Chicago, IL) on all observed data.

RESULTS

Pressure and Cold Denaturation of SHa rPrP(90−231) Revealed from ^{1}H and $^{1}H-^{15}N$ HSQC NMR Spectra. The effect of pressure on the ^{1}H NMR spectrum of rPrP(90−231) at pH 5.2 and 30 °C is shown in Figure 1a−c. At 30 °C and 30 bar, the spectrum is that of the folded native structure (Figure 1a). With increasing pressure, the spectral pattern changes gradually. In particular, the methyl proton signals at high field, arising from I182 (helix B) and L130 (strand S1), marked with one and two asterisks, respectively, disappear almost completely at 2500 bar (Figure 1c). This observation indicates that the tertiary structure surrounding these residues is collapsed at high pressure. Apparently, however, the entire core is not destroyed at 2500 bar, since the spectrum at 2500 bar is not completely that of random coil (cf. Figure 1f), but retains some structural features. Therefore, the spectral changes may be considered to represent a change in the conformational equilibrium between the native structure (N) and an intermediate structure (I) (see eq 1), the equilibrium of which varies with pressure according to eq 3. Figure 4a plots the intensities of those two methyl proton signals as a function of pressure. Curve

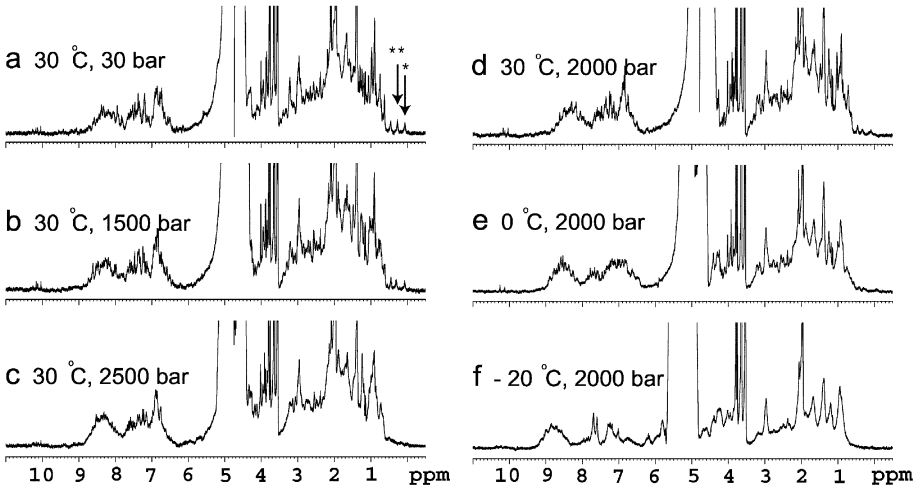

FIGURE 1: NMR spectra of rPrP(90−231) as a function of pressure at 30 °C and pH 5.2. (a−c) 1D proton NMR spectra, demonstrating the change from being characteristic of the native protein to "substantially unfolded" with increasing hydrostatic pressure. One asterisk and two asterisks denote signals of Hγ12 and/or Hγ13 of I182 (helix B) and Hδ1 and/or Hδ2 of L130 (strand S1), respectively (*7*, *9*), both in the hydrophobic core. (d−f) Spectra at 2000 bar with decreasing temperature, showing cold denaturation.

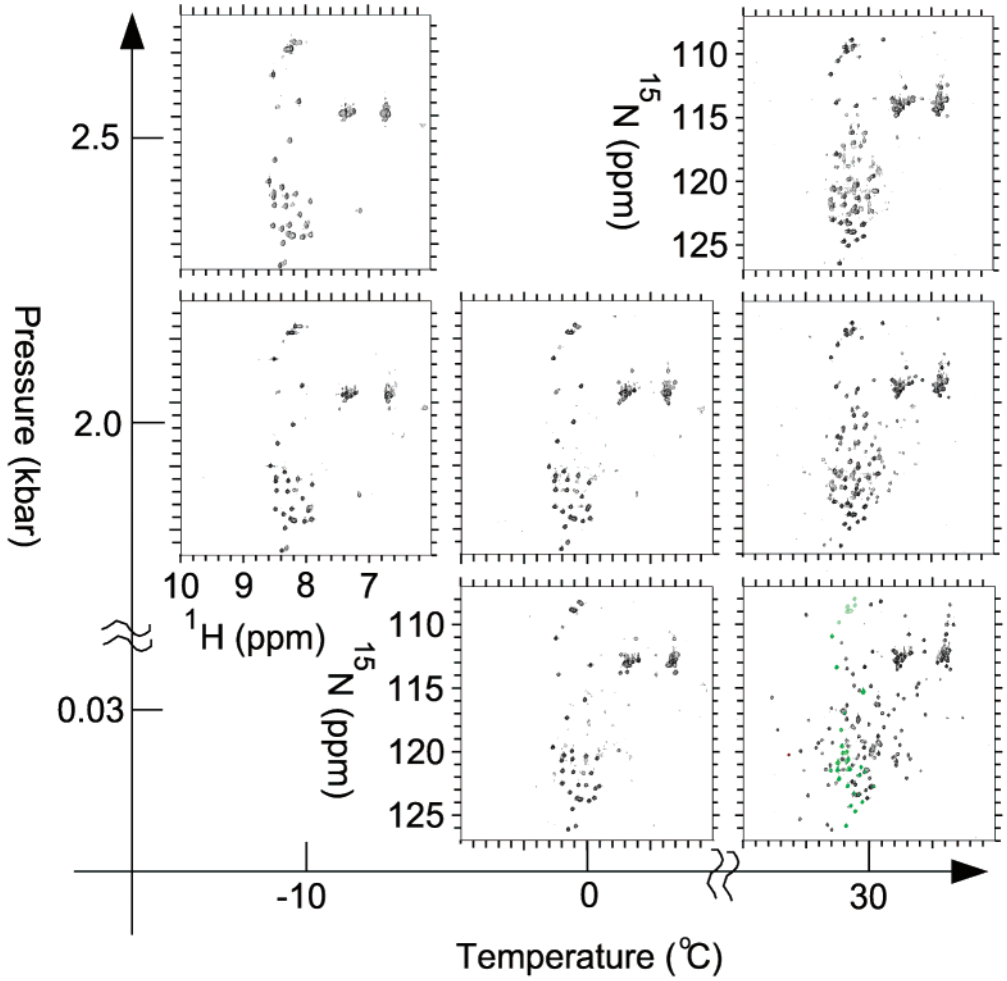

FIGURE 2: ^{1}H−^{15}N HSQC spectra of rPrP(90−231) as a function of pressure and temperature. Signals from residues 90−128 are colored green in the spectrum at 30 bar, 30 °C, and pH 5.2. With an increase in pressure or a decrease in temperature, amide cross-peaks from the core region that are clearly observed in the native state at 30 bar and 30 °C diminished in magnitude and almost disappeared at 2500 bar and 30 °C and at 30 bar and 0 °C, illustrating pressure and cold denaturation, respectively. Signals from the N-terminal and hydrophobic cluster (residues 90−128, colored green) remain unchanged even at 2500 bar and −10 °C.

fitting using eqs 1−3 in Materials and Methods gives free energy (ΔG_0) and molar volume (ΔV_0) differences of 3.1 kcal/mol and −80 mL/mol, respectively (as the average for the two signals), at pH 5.2, 30 °C, and 1 bar.

Figure 1d−f shows spectral changes at 2000 bar as a function of temperature. Above 30 °C and ambient pressure, the protein starts to aggregate, prohibiting measurements at higher temperatures. Interestingly, cooling the solution

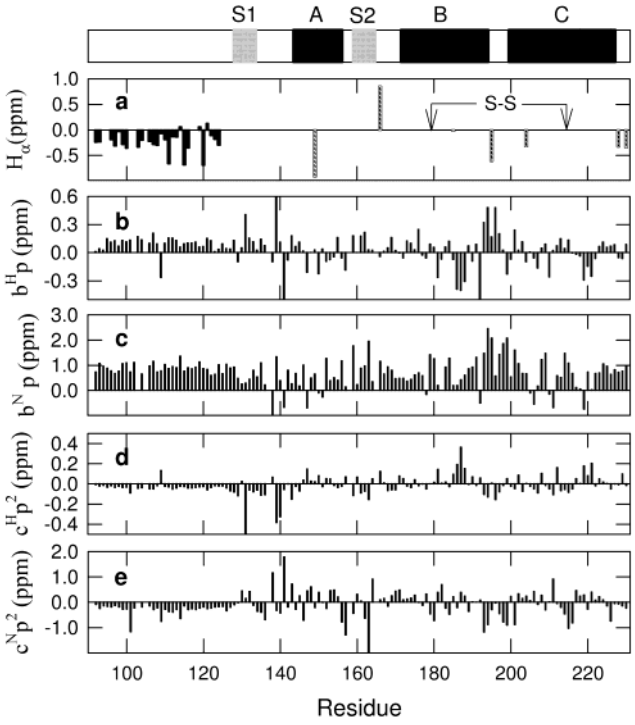

FIGURE 3: Pressure and temperature dependence of chemical shifts. (a) H_α chemical shift deviations from random coil values for rPrP(90−231) at 2 °C and pH 5.2. The segment from residue 92 to 124 evidently has many short transient helices. Only those residues from the C-terminal region with a hatched bar can be observed. (b−e) Decomposition of the pressure dependence of amide proton and ^{15}N shifts, at 30 °C, into linear and quadratic terms (see eq 4 in Materials and Methods). (b) Linear component of the ^1H chemical shift pressure dependence, $b^H \times 2500$, as a function of residue number. (c) Linear component of the ^{15}N chemical shift pressure dependence, $b^N \times 2500$. (d) Nonlinear component of the ^1H chemical shift pressure dependence, $c^H \times 2500^2$. (e) Nonlinear component of the ^{15}N chemical shift pressure dependence, $c^N \times 2500^2$.

changed the spectral pattern dramatically and at −20 °C gave the pattern of Figure 1f, which is clearly that of a fully unfolded protein. The observation shows that rPrP(90−231) underwent cold denaturation at 2000 bar.

Figure 2 shows changes in $^1H-^{15}N$ heteronuclear single-quantum coherence (HSQC) spectra of uniformly ^{15}N-labeled rPrP(90−231) at various pressures and temperatures. With increases in pressure, the intensities of amide $^1H-^{15}N$ cross-peaks from the core region (residues 128−231) that are dispersed at 30 bar and 30 °C in the native state diminished and nearly (but not entirely) disappeared at 2500 bar and 30 °C, leaving cross-peaks in only a narrow range of chemical shifts (7.8−8.6 ppm for ^1H). The chemical shift range of these broad and apparently overlapped cross-peaks is coincident with those from the naturally disordered N-terminal segment and the hydrophobic cluster (*7*, *9*), i.e., from residues 90−127, which are colored green. The other signals in this range emanate from the rest of the protein which is unfolded under pressure. A similar spectral change with loss of dispersed cross-peaks was also observed by lowering the temperature to 0 °C at 30 bar, suggesting that cold denaturation also takes place at 30 bar. The loss of the dispersed signals is almost complete below −10 °C at 2000 bar, suggesting a more complete cold denaturation at lower temperatures and high pressures.

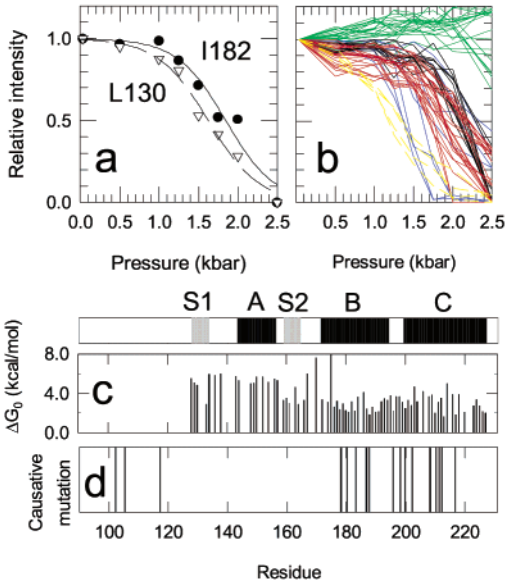

FIGURE 4: (a) Integral signal intensities of Hγ12 and/or Hγ13 of I182 (−) and Hδ1 and/or Hδ2 of L130 (− − −) in 1D ^1H NMR spectra of rPrP(90−231) measured at 30 °C and pH 5.2 as a function of pressure. Nonlinear curve fitting (eqs 1−3; see Materials and Methods) yielded values of ΔG_0, ΔV, $\Delta\beta$, and P_m for I182 of 3.16 kcal/mol, −83.2 mL/mol, 4.33×10^{-16} mL^2 dyn^{-1} cm^{-1}, and 1850 bar and for L130 of 3.05 kcal/mol, −80.4 mL/mol, 1.23×10^{-16} mL^2 dyn^{-1} cm^{-1}, and 1630 bar, respectively. (b) Relative HSQC cross-peak intensities for individual amides as a function of pressure at 30 °C. Intensities of the residues at the N-terminal region (residues 90−112) and hydrophobic cluster (residues 113−121) are colored green. Strand S1 (residues 128−133) and S2 (residues 159−164) intensities are colored blue. S1−A loop (residues 134−143) and helix A (residues 144−154) intensities are colored black. Helix B (residues 172−193) and helix C (residues 200−227) intensities are colored red. Residues V210, M213, Q217, and K220 forming the interface between strand S1 and S2 in helix C are shown in dotted lines in yellow (ΔG_0 on average, 2.1 ± 0.2 kcal/mol, −75 ± 5, 1220 ± 20 bar). (c) Plot of ΔG_0 as a function of residue number. (d) Point mutations associated with known human prion diseases (*34*) (P102L, P105L, A117V, D178N, V180I, T183A, H187R, T188R, E196K, F198S, E200K, D202N, R208H, V210I, E211Q, Q212P, and Q217R).

The Disordered N-Terminal Region Has Nascent Helices. At all the pressures that were employed, the N-terminal residues (90−127) gave amide proton chemical shifts in a narrowly confined region of 7.8−8.6 ppm, indicating that residues 90−127 are largely disordered (Figure 2). To discover more details about the conformational preferences in this region, we measured H_α chemical shifts in the TOCSY-HSQC and NOESY-HSQC spectra at 2 °C and 1 bar (spectra not shown) in a regular 5 mm sample tube, because of the limited sample volume of the high-pressure cell. At 2 °C, C-terminal signals were broadened beyond detection, and only residues 90−127 gave clearly detectable signals similar to those at 2500 bar and 30 °C. We found that the H_α chemical shifts for the N-terminal segment and the hydrophobic cluster are appreciably shifted upfield from random coil values (Figure 3a), suggesting that the N-terminal segment and hydrophobic cluster consist of short, transient helices. In this context, we note that a 56-residue peptide comprising PrP residues 90−145 can form helices or intermolecular β-sheets, depending on its microenvironment (*25*).

Conformational Fluctuations within the Folded Manifold Revealed with Pressure Shifts. Before major changes in

cross-peak intensities in the HSQC spectrum occur with increasing pressure at 30 °C, amide ^{1}H and ^{15}N signals showed pressure-dependent shifts, which were reversible with pressure. By plotting the chemical shifts of individual amide ^{1}H and ^{15}N signals separately, we found that their shifts are considerably nonlinear with pressure, indicative of conformational changes before the onset of unfolding (*22*). We separated linear and nonlinear components of the chemical shift changes with pressure for each amide ^{1}H or ^{15}N signal according to eq 4 in Materials and Methods, and plotted them in Figures 3b−e. While the magnitudes of the signals were considerably diminished at high pressures, there was sufficient signal to determine chemical shifts in most cases.

Linear components of shifts generally correspond to small structural fluctuations of the backbone at 1 bar, whereas nonlinear components correspond to nonlinear structural changes involving excursion to a higher-energy conformation within the folded manifold, the population of which increases at higher pressures (*16*). Furthermore, whereas the amide ^{1}H shift (Figure 3b,d) monitors the hydrogen bonding state of the backbone, the amide ^{15}N shift (Figure 3c,e) is more sensitive to changes in local torsion angles (*18*). All amide ^{1}H signals of PrP shifted to lower field (i.e., positive shift) with pressure, indicating general shrinking of hydrogen bonds. The relatively large and nearly linear low-field shifts with monotonic variations with amino acid sequence in the N-terminal region (residues 90−127) for both ^{1}H (average $b^Hp = 0.086 \pm 0.079$ at 2500 bar) and ^{15}N (average $b^Np = 0.90 \pm 0.02$) support the notion that these amide groups are exposed to the solvent, meaning that the region has no particular tertiary structure (*26*). In contrast, larger variations in b^Hp and b^Np are confined to the rest of the polypeptide chain (residues 128−231), suggesting heterogeneous fluctuations of the backbone for this region of the protein. Anomalous b^Hp values are centered around residues 138−141 (S1-A loop) and residues 181−199 (the C-terminal half of helix B and the B−C loop), suggesting that these secondary structure segments undergo significant conformational changes within the native fold.

Excursion of the protein conformation beyond the basic native structure, which typically occurs in <1 ms, is manifested in nonlinear pressure shifts (*21*, *22*). Anomalously large nonlinear ^{1}H shifts are found in the S1 strand (G131), the S1−A loop (M139 and H140), and the C-terminal half of helix B (H187). Anomalous nonlinear ^{15}N shifts are mostly found in loop regions: S1−A loop (M138 and F141), A−S2 loop (Y157), and B−C loop (T199), suggesting nonlinear torsion angle alterations, or possibly hinge motions, in the polypeptide backbone localized around these residues. The locations of these residues exhibiting nonlinear pressure shifts are shown by blue colors in the structure of PrP^C in Figure 5a.

Locally Disordered Intermediate Revealed from HSQC Cross-Peak Intensities. The well-dispersed ^{1}H−^{15}N HSQC cross-peaks from the core moiety disappear with a further increase in pressure (Figure 2). Loss of their intensities is partly compensated by the appearance of new signals corresponding to random coil by 2500 bar, but most signals are lost. In a globular protein with a relatively high molecular weight, loss of HSQC cross-peaks by pressure occurs rather generally due to broadening of signals from heterogeneously disordered segments (*21*). The broadening could arise from insufficient time averaging of the chemical shift heterogeneity of the randomly oriented amide groups of the disordered polypeptide chain due to its restricted mobility (with time constants on the order of microseconds to milliseconds). The mechanism is the same as that proposed for the loss of HSQC cross-peaks in a typical molten globule produced at low pH (*27*). Irrespective of whether one observes the appearance of new signals, the loss of pre-existing signals indicates that the exchange between the pre-existing species and the newly produced species is slow on the NMR time scale (faster than milliseconds). In this case, each integrated cross-peak intensity, normalized to that at 1 bar, represents the fraction of the folded conformer monitored at each amino acid residue (*28*).

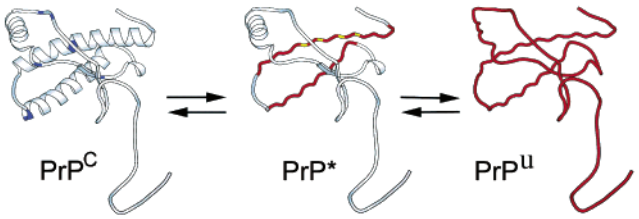

FIGURE 5: Schematic representation of three major conformers of SHa rPrP(90−231), the native protein PrP^C, the major intermediate conformer PrP*, and the unfolded conformer PrP^U, based on the NMR structure of PrP^C (*7*, *9*). Their populations at equilibrium at pH 5.2, 30 °C, and 1 bar are estimated to be ~99, ~1, and ~0.01%, respectively. In PrP^C, blue represents residues with anomalous nonlinear ^{15}N shifts (M138, F141, Y157, Y163, T193, and E211), suggesting nonlinear torsion angle changes or possibly hinge motions in the polypeptide backbone. In PrP*, disordered helices B and C are colored red. Particularly unstable residues in helix C (V210, M213, Q217, and K220), where $\Delta G_0 \sim 2.1$ kcal/mol on average, are colored yellow.

Figure 4b represents the ^{1}H−^{15}N HSQC cross-peak intensities (normalized at 30 bar) of all individual residues of the folded conformer as a function of pressure.

Only the cross-peak intensities from the N-terminal segment (residues 90−112) and hydrophobic cluster (residues 113−127) (Figure 4b, green) are nearly invariant with pressure, but all other peak intensities decrease with pressure. Interestingly, the transition curve varies from site to site, showing that the local conformational stability of rPrP(90−231) is site-dependent. The relative inertness of the N-terminal segment to pressure is a general property of a disordered conformer (*26*).

We performed curve fitting of ΔG against pressure for individual residues using eqs 1−3 under the assumption that individual residues undergo two-state transitions. By extrapolating the plots to 1 bar, we determined thermodynamic stabilities ΔG_0 for individual residues at pH 5.2, 30 °C, and 1 bar (Figure 4c). The most interesting result in Figure 4c is that the stabilities of helices B and C are distinctly low, their average stabilities being 3.0 and 3.1 kcal/mol, respectively. Helices B and C are near a cluster of cavities, suggesting that the selective disorder of helices B and C is related to the deformation and collapse of these cavities. On the other hand, helix A is much more stable, giving a ΔG_0 of 5.3 kcal/mol. Stabilities of S1 and S2 and the surrounding loops are considerably heterogeneous within their constituting residues, and their average stabilities rank between those of helix A and helices B and C (Figure 4b, blue). The heterogeneous stability of the loop regions is consistent with the existence

of nonlinear local motions (possibly hinge motions) within the folded state inferred from nonlinear ^{15}N shifts.

Transitions of residues in helix C (200−227) also occurred quite heterogeneously at pressures between 500 and 2500 bar. Unusually unstable residues are V210, M213, Q217, and K220, which are shown with yellow dotted lines in Figure 4b. Thermodynamic analysis, extrapolated to 1 bar via eq 3, gave a ΔG_0 value of 2.1 kcal/mol on average. These residues are located essentially at the interface with β-strands S1 and S2 (see residues in yellow of PrP* in Figure 5), suggesting that broadening arises from local disorder in the relative orientation of strands S1 and S2, independent of the total disorder or melting of helices B and C. Intriguingly, recent X-ray analysis (*29*) showed domain swapping of helix C in the dimeric state of prion protein. Although the mechanism of disulfide swapping is unknown, the mutual orientational instability of helices B and C may contribute to this reaction.

Previously reported values of ΔG_0 for unfolding PrP using denaturants under various conditions (pH 4.0−8.0 and temperature of 4−30 °C) were between 7.0 and 8.5 kcal/mol (*24*, *30*−*32*), i.e., greater than those determined from the present experiments for helix A (5.3 kcal/mol). The stability of PrP^C remains almost unchanged between pH 5.0 and 7.0, and the unfolding intermediate is observable only at pH <4.5 at 22.0 °C (*32*). Unfolding of SHa rPrP(90−231) with guanidinium chloride, however, revealed under certain conditions an intermediate state only 1.9 kcal/mol less stable than the native folded state, in qualitative agreement with the present result (*24*).

In conclusion, the variable thermodynamic stabilities demonstrated for different secondary structure elements and even within these elements indicate that PrP^C exists in an equilibrium of multiple conformers under roughly physiological solution conditions. If the heterogeneous stability within helix C is disregarded, there are at least three major conformers in equilibrium: the folded conformer PrP^C with heterogeneous fluctuations in the backbone, particularly in the loop regions, an intermediate folded conformer with selectively disordered helices B and C, and the totally unfolded conformer. The rates of exchange among them are slow ($<10^3\ s^{-1}$). The ΔG_0 values corresponding to the change from the native state to the metastable intermediate (unfolded B and C helices) and between the native state and the unfolded species (unfolded A−C helices) can be calculated from the averages of each individual residue in each secondary structural moiety. From the ΔG_0 values, their populations are estimated using Boltzmann's equation to be approximately 99, 1, and 0.01%, respectively, at pH 5.2, 30 °C, and 1 bar. As we have incrementally increased the pressure from 1 to 2500 bar, we have observed spectra from the folded conformer (with the largest partial molar volume) to the totally unfolded conformer (with the smallest partial molar volume). Consequently, other than those detected in the work presented here, no major intermediate conformers are likely to be present in SHa rPrP(90−231) under conditions approximating physiological conditions. If the intermediate detected here at a population of ~1% of the total PrP is not precisely PrP*, then the population of PrP* must be much smaller than that of the intermediate we have identified. Even if that was the case, PrP* should have many of the same characteristics as the identified intermediate.

DISCUSSION

The putative form of PrP that interacts with PrP^{Sc} in the transformation to the infectious form (vide supra), namely, PrP*, is considered to coexist with native PrP^C under physiological conditions (*13*). Our high-pressure NMR experiments showed that the intermediate conformer with disordered helices B and C is the only major non-native conformer in SHa rPrP(90−231) under roughly physiological conditions (pH 5.2 and 30 °C), and our previous studies showed that the same native structure prevailed at pH 7 (*7*). A similar intermediate can be expected to be present in the intact PrP^C. We may most logically identify the intermediate with PrP* itself, or otherwise, with a closely related precursor to PrP*. The disordered helices B and C of the metastable intermediate may, through intermolecular association with the template presented by the β-sheet structure of multimolecular PrP^{Sc}, facilitate the $PrP^C \rightarrow PrP^{Sc}$ transformation.

Available immunological and pathological information to date also supports the notion that the intermediate conformer found in this work be identified with PrP*. First, the region of helices B and C shown to be disordered corresponds to a discontinuous epitope for binding of a species-specific agent, provisionally termed protein X, which apparently functions as a molecular chaperone in conversion of PrP^C to PrP^{Sc} (*33*). We can speculate that the conformational disorder in the region facilitates protein X binding. Second, many point mutations associated with inherited human prion diseases are either within or adjacent to regions of helices B and C (*34*). It is intriguing to find that the region of instability coincides with the region where most causal mutations have been found (Figure 4d). Such mutations could further decrease the stability of helices B and C, increasing the equilibrium population of the reactive intermediate, thereby increasing the chance of the formation of PrP^{Sc}.

An additional surprising finding in this work is that the conformational stability of SHa rPrP(90−231) decreases substantially at low temperatures; namely, the protein undergoes cold denaturation even under approximately physiological conditions (pH 5.2). Since the low stability at low temperatures must be an intrinsic design of the prion protein, the finding suggests an interesting possibility that the instability at low temperatures is related to the biological function and possibly to the pathogenesis of prion protein.

NOTE ADDED AFTER ASAP POSTING

This paper was inadvertently posted 09/18/2002. Equation 3 has been modified, and the correct version of the paper was posted 10/08/2002.

ACKNOWLEDGMENT

We thank Drs. Ryo Kitahara, He Liu, and Davide Tonelli for aid with this study and Dr. Seiichi Era for support.

SUPPORTING INFORMATION AVAILABLE

^1H and ^{15}N chemical shifts as a function of pressure. This material is available free of charge via the Internet at http://pubs.acs.org.

REFERENCES

1. Jackson, G. S., and Clarke, A. R. (2000) *Curr. Opin. Struct. Biol. 10*, 69−74.
2. Stahl, N., Baldwin, M. A., Teplow, D. B., Hood, L., Gibson, B. W., Burlingame, A. L., and Prusiner, S. B. (1993) *Biochemistry 32*, 1991−2002.
3. Caughey, B. W., Dong, A., Bhat, K. S., Ernst, D., Hayes, S. F., and Caughey, W. S. (1991) *Biochemistry 30*, 7672−7680.
4. Pan, K.-M., Baldwin, M., Nguyen, J., Gasset, M., Serban, A., Groth, D., Mehlhorn, I., Huang, Z., Fletterick, R. J., Cohen, F. E., and Prusiner, S. B. (1993) *Proc. Natl. Acad. Sci. U.S.A. 90*, 10962−10966.
5. Prusiner, S. B., Bolton, D. C., Groth, D. F., Bowman, K. A., Cochran, S. P., and McKinley, M. P. (1982) *Biochemistry 21*, 6942−6950.
6. Riek, R., Hornemann, S., Wider, G., Billeter, M., Glockshuber, R., and Wüthrich, K. (1996) *Nature 382*, 180−182.
7. James, T. L., Liu, H., Ulyanov, N. B., Farr-Jones, S., Zhang, H., Donne, D. G., Kaneko, K., Groth, D., Mehlhorn, I., Prusiner, S. B., and Cohen, F. E. (1997) *Proc. Natl. Acad. Sci. U.S.A. 94*, 10086−10091.
8. Donne, D. G., Viles, J. H., Groth, D., Mehlhorn, I., James, T. L., Cohen, F. E., Prusiner, S. B., Wright, P. E., and Dyson, H. J. (1997) *Proc. Natl. Acad. Sci. U.S.A. 94*, 13452−13457.
9. Liu, H., Farr-Jones, S., Ulyanov, N. B., Llinas, M., Marqusee, S., Groth, D., Cohen, F. E., Prusiner, S. B., and James, T. L. (1999) *Biochemistry 38*, 5362−5377.
10. Lopez Garcia, F., Zahn, R., Riek, R., and Wuthrich, K. (2000) *Proc. Natl. Acad. Sci. U.S.A. 97*, 8334−8339.
11. Zahn, R., Liu, A. Z., Luhrs, T., Riek, R., von Schroetter, C., Garcia, F. L., Billeter, M., Calzolai, L., Wider, G., and Wuthrich, K. (2000) *Proc. Natl. Acad. Sci. U.S.A. 97*, 145−150.
12. Prusiner, S. B., Scott, M., Foster, D., Pan, K.-M., Groth, D., Mirenda, C., Torchia, M., Yang, S.-L., Serban, D., Carlson, G. A., Hoppe, P. C., Westaway, D., and DeArmond, S. J. (1990) *Cell 63*, 673−686.
13. Cohen, F. E., Pan, K.-M., Huang, Z., Baldwin, M., Fletterick, R. J., and Prusiner, S. B. (1994) *Science 264*, 530−531.
14. Kocisko, D. A., Come, J. H., Priola, S. A., Chesebro, B., Raymond, G. J., Lansbury, P. T., and Caughey, B. (1994) *Nature 370*, 471−474.
15. Kaneko, K., Peretz, D., Pan, K. M., Blochberger, T. C., Wille, H., Gabizon, R., Griffith, O. H., Cohen, F. E., Baldwin, M. A., and Prusiner, S. B. (1995) *Proc. Natl. Acad. Sci. U.S.A. 92*, 11160−11164.
16. Akasaka, K., and Yamada, H. (2001) in *Methods in Enzymology* (James, T. L., Dötsch, V., and Schmitz, U., Eds.) pp 134−158, Academic Press, San Diego.
17. Yamada, H. (1974) *Rev. Sci. Instrum. 45*, 640−642.
18. Akasaka, K., Li, H., Yamada, H., Li, R. H., Thoresen, T., and Woodward, C. K. (1999) *Protein Sci. 8*, 1946−1953.
19. Kitahara, R., Yamada, H., and Akasaka, K. (2001) *Biochemistry 40*, 13556−13563.
20. Orekhov, V. Y., Dubovskii, P. V., Yamada, H., Akasaka, K., and Arseniev, A. S. (2000) *J. Biomol. NMR 17*, 257−263.
21. Kuwata, K., Li, H., Yamada, H., Batt, C. A., Goto, Y., and Akasaka, K. (2001) *J. Mol. Biol. 305*, 1073−1083.
22. Akasaka, K., and Li, H. (2001) *Biochemistry 40*, 8665−8671.
23. Kitahara, R., Sareth, S., Yamada, H., Ohmae, E., Gekko, K., and Akasaka, K. (2000) *Biochemistry 39*, 12789−12795.
24. Zhang, H., Stöckel, J., Mehlhorn, I., Groth, D., Baldwin, M. A., Prusiner, S. B., James, T. L., and Cohen, F. E. (1997) *Biochemistry 36*, 3543−3553.
25. Zhang, H., Kaneko, K., Nguyen, J. T., Livshits, T. L., Baldwin, M. A., Cohen, F. E., James, T. L., and Prusiner, S. B. (1995) *J. Mol. Biol. 250*, 514−526.
26. Kamatari, Y. O., Yamada, H., Akasaka, K., Jones, J. A., Dobson, C. M., and Smith, L. J. (2001) *Eur. J. Biochem. 268*, 1782−1793.
27. Redfield, C., Schulman, B. A., Milhollen, M. A., Kim, P. S., and Dobson, C. M. (1999) *Nat. Struct. Biol. 6*, 948−952.
28. Inoue, K., Yamada, H., Akasaka, K., Hermann, C., Kremer, W., Maurer, T., Doker, R., and Kalbitzer, H. R. (2000) *Nat. Struct. Biol. 7*, 547−550.
29. Knaus, K. J., Morillas, M., Swietnicki, W., Malone, M., Surewicz, W. K., and Yee, V. C. (2001) *Nat. Struct. Biol. 8*, 770−774.
30. Wildegger, G., Liemann, S., and Glockshuber, R. (1999) *Nat. Struct. Biol. 6*, 550−553.
31. Hosszu, L. L. P., Baxter, N. J., Jackson, G. S., Power, A., Clarke, A. R., Waltho, J. P., Craven, C. J., and Collinge, J. (1999) *Nat. Struct. Biol. 6*, 740−743.
32. Hornemann, S., and Glockshuber, R. (1998) *Proc. Natl. Acad. Sci. U.S.A. 95*, 6010−6014.
33. Kaneko, K., Zulianello, L., Scott, M., Cooper, C. M., Wallace, A. C., James, T. L., Cohen, F. E., and Prusiner, S. B. (1997) *Proc. Natl. Acad. Sci. U.S.A. 94*, 10069−10074.
34. Prusiner, S. B. (1996) *Curr. Top. Microbiol. Immunol. 207*, 1−17.

BI026129Y